jmb Article

# Serine Phosphorylation Suppresses Huntingtin Amyloid Accumulation by Altering Protein Aggregation Properties

Rakesh Mishra[1,2], Cody L. Hoop[1], Ravindra Kodali[1,2], Bankanidhi Sahoo[1,2], Patrick C. A. van der Wel[1] and Ronald Wetzel[1,2]

*1 - **Department of Structural Biology,** University of Pittsburgh School of Medicine, Pittsburgh, PA 15260, USA*
*2 - **Pittsburgh Institute for Neurodegenerative Diseases,** University of Pittsburgh School of Medicine, Pittsburgh, PA 15260, USA*

***Correspondence to Ronald Wetzel:** Rm. 2046, Biomedical Sciences Tower 3, 3501 Fifth Avenue, Pittsburgh, PA 15260, USA. rwetzel@pitt.edu*
http://dx.doi.org/10.1016/j.jmb.2012.09.011
***Edited by J. Weissman***

## Abstract

Aggregation of expanded polyglutamine repeat-containing fragments of the huntingtin (htt) protein may play a key role in Huntington's disease. Consistent with this hypothesis, two Ser-to-Asp mutations in the 17-amino-acid N-terminal $htt^{NT}$ segment abrogate both visible brain aggregates and disease symptoms in a full-length $Q_{97}$ htt mouse model while compromising aggregation kinetics and aggregate morphology in an htt fragment *in vitro* [Gu *et al.* (2009). Serines 13 and 16 are critical determinants of full-length human mutant huntingtin induced disease pathogenesis in HD mice. *Neuron* **64**, 828–840]. The $htt^{NT}$ segment has been shown to play a critical role in facilitating nucleation of amyloid formation in htt N-terminal exon1 fragments. We show here how these Ser-to-Asp mutations dramatically affect aggregation kinetics and aggregate structural integrity. First, these negatively charged Ser replacements impair the assembly of the α-helical oligomers that play a critical role in htt amyloid nucleation, thus providing an explanation for reduced amyloid formation rates. Second, these sequence modifications alter aggregate morphology, decrease aggregate stability, and enhance the steric accessibility of the $htt^{NT}$ segment within the aggregates. Together, these changes make the sequence-modified peptides kinetically and thermodynamically less likely to aggregate and more susceptible, if they do, to posttranslational modifications and degradation. These effects also show how phosphorylation of a protein might achieve cellular effects *via* direct impacts on the protein's aggregation properties. In fact, preliminary studies on exon1-like molecules containing phosphoryl-Ser residues at positions 13 and 16 show that they reduce aggregation rates and generate atypical aggregate morphologies similar to the effects of the Ser-to-Asp mutants.

© 2012 Elsevier Ltd. All rights reserved.

## Introduction

Huntington's disease (HD)[1,2] is one of 10[3,4] CAG repeat diseases characterized by the expansion of a polyglutamine (polyQ) stretch in a particular protein. In HD, this polyQ stretch begins at amino acid 18 of the ~3200-amino-acid-long huntingtin (htt) protein. A hallmark feature of this disease is the presence of ubiquitinylated, aggregated forms of htt fragments in neurons of disease victims and in animal and cell models.[5,6] Additional evidence of a disease role for protein aggregation and/or misfolding comes from observations that disease risk[3] and *in vitro* aggregation rates[7,8] both increase with polyQ repeat expansion, as well as from the temporal association of aggregate formation and disease symptoms in some model organisms.[1] The precise identities and immediate cellular targets of these implicated toxic, aberrantly folded forms of htt have not been identified.

A dramatic example of the association of brain aggregates with HD symptoms was described by Gu *et al.*[9] This group previously constructed a tg mouse containing a $Q_{97}$ form of full-length htt that exhibited accumulation of cortical and striatal aggregates and HD-like neurological deficits.[10] In subsequent work,

| Name | Sequence |
|---|---|
| Human htt exon 1 | MATLEKLMKA FESLKSF--- QQQQQQQQQQ QQQQQQQQQQ QQQQQQQQQQ QQQQQ----- PPPPPPPPPP-Htt-C[a] |
| $htt^{NT}$ | MATLEKLMKA FESLKSF |
| $htt^{NT}Q_3$ | MATLEKLMKA FESLKSF--- QQQ |
| $htt^{NT}Q_8K_2$ (F17W) | MATLEKLMKA FESLKSW--- QQQQQQQQKK |
| $htt^{NT}Q_8K_2$ (F17W/S13D/S16D) | MATLEKLMKA FEDLKDW--- QQQQQQQQKK |
| $htt^{NT}Q_{30}P_{10}K_2$ (S13D/S16D) | MATLEKLMKA FEDLKDF--- QQQQQQQQQQ QQQQQQQQQQ QQQQQQQQQQ ---------- PPPPPPPPPP KK |
| $htt^{NT}Q_{37}P_{10}K_2$ (F17W) | MATLEKLMKA FESLKSW--- QQQQQQQQQQ QQQQQQQQQQ QQQQQQQQQQ QQQQQQQ--- PPPPPPPPPP KK |
| $htt^{NT}Q_{37}P_{10}K_2$ (F17W/S13D/S16D) | MATLEKLMKA FEDLKDW--- QQQQQQQQQQ QQQQQQQQQQ QQQQQQQQQQ QQQQQQQ--- PPPPPPPPPP KK |
| $htt^{NT}Q_{37}P_{10}K_2$(¥-1/F17W) | ¥MATLEKLMK AFESLKSW-- QQQQQQQQQQ QQQQQQQQQQ QQQQQQQQQQ QQQQQQQ--- PPPPPPPPPP KK |
| $htt^{NT}Q_{37}P_{10}K_2$(¥-1/F17W/S13D/S16D | ¥MATLEKLMK AFEDLKDW-- QQQQQQQQQQ QQQQQQQQQQ QQQQQQQQQQ QQQQQQQ--- PPPPPPPPPP KK |
| $htt^{NT}Q_{37}P_{10}K_2$ (F17W/S13§/S16§) | MATLEKLMKA FE§LK§W--- QQQQQQQQQQ QQQQQQQQQQ QQQQQQQQQQ QQQQQQQ--- PPPPPPPPPP KK |
| $htt^{NT}Q_{37}P_{10}K_2$ (F17W/S13§) | MATLEKLMKA FE§LKSW--- QQQQQQQQQQ QQQQQQQQQQ QQQQQQQQQQ QQQQQQQ--- PPPPPPPPPP KK |
| $htt^{NT}Q_{37}P_{10}K_2$ (F17W/S16§) | MATLEKLMKA FESLK§W--- QQQQQQQQQQ QQQQQQQQQQ QQQQQQQQQQ QQQQQQQ--- PPPPPPPPPP KK |
| $PGQ_9P^{1,2,3}K_8$ | QQQQPQQQQP GQQQQPQQQQ PGQQQQPQQQ QPGQQQQQQQQ QQKKKKKKKK |

[a]Htt-C = PQLPQPPPQA QPLLPQPQPP PPPPPPPPGP AVAEEPPLHR P; § = phosphoryl-Ser; ¥ = Glu-EDANS

**Fig. 1.** Amino acid sequences of the peptides studied.

an identical $Q_{97}$ construct containing phosphomimetic Ser→Asp point mutations at positions 13 and 16 exhibited no disease symptoms and no accumulated visible aggregates.[9] Although these effects might be accounted for *via* possible cell targeting functions of the N-terminal $htt^{NT}$ sequence[11–15] (Fig. 1), we speculated[9] that these Ser-to-Asp mutations could also alter the physical properties of cellular htt fragments, especially in the context of misfolding and aggregation. Consistent with this, we showed in that paper that the same mutations in a polyQ-containing htt fragment model peptide slow *in vitro* aggregation rates and yield significantly different aggregate morphologies.[9] How the conversion

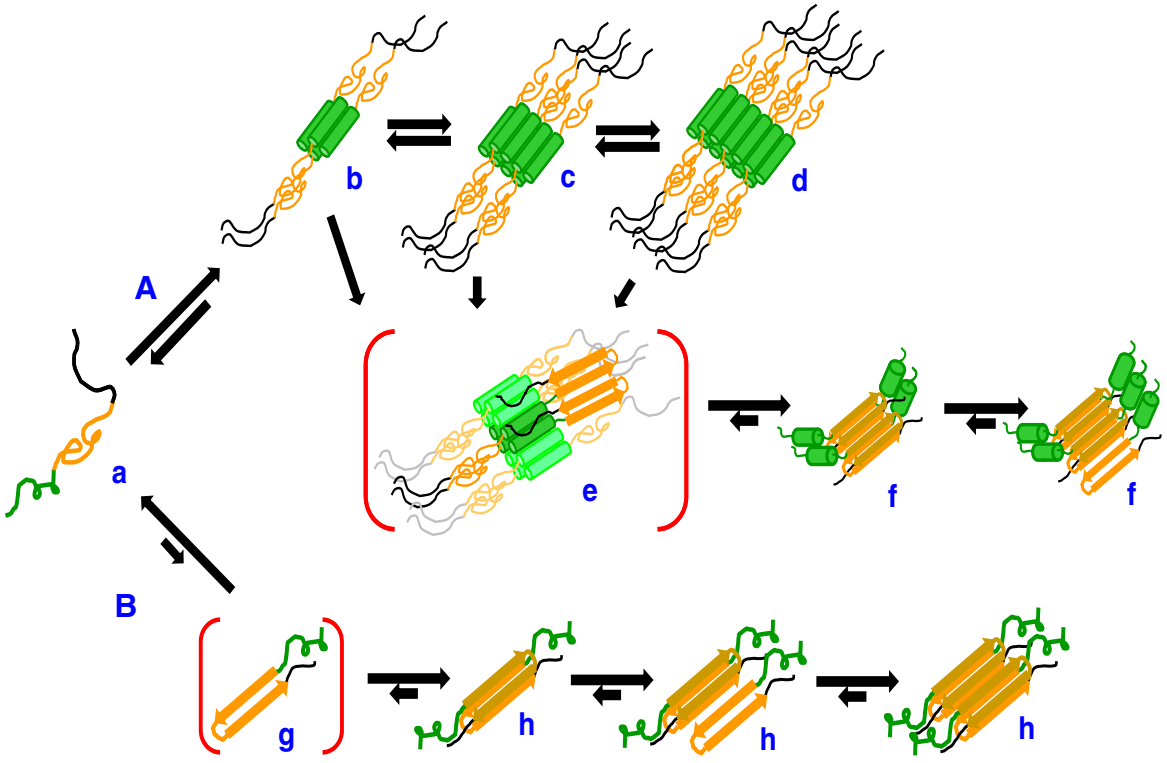


**Fig. 2.** Schematic model of htt fragment aggregation mechanisms. PolyQ-containing htt fragments (a; $htt^{NT}$, green; polyQ, orange; Pro-rich, black) can undergo nucleation of polyQ amyloid formation in two ways. In path A, $htt^{NT}$ segments undergo reversible formation of α-helical tetramers (b) and higher oligomers (c and d) whose disordered polyQ elements can interact to nucleate amyloid structure (e) and grow by monomer addition (f). In path B, the polyQ segment of monomeric htt fragments (a) can directly undergo reversible assembly into a critical nucleus (g) followed by elongation into amyloid (h). The conformation of $htt^{NT}$ within the B pathway aggregates has not been determined.

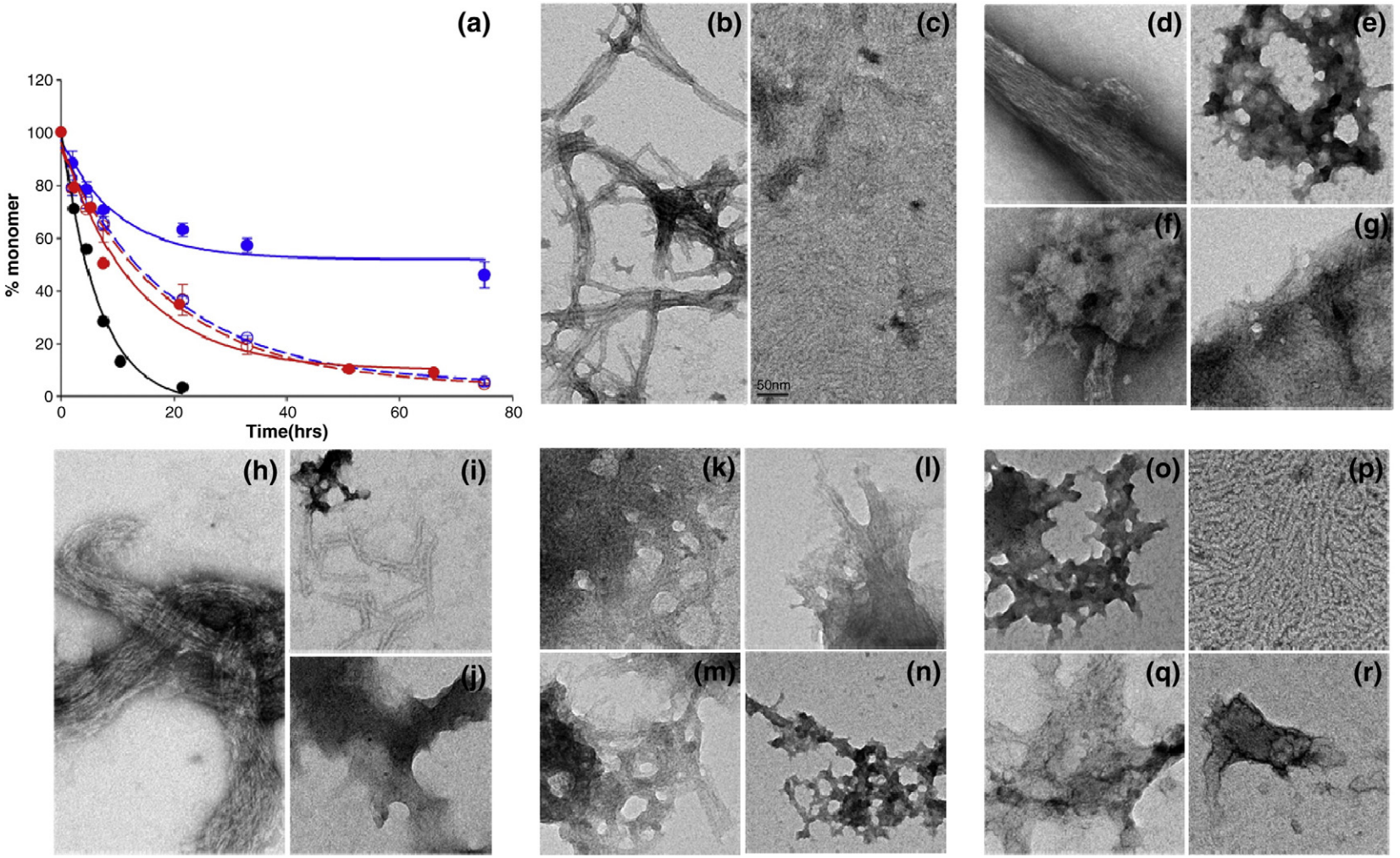


**Fig. 3.** Aggregation of Ser-modified derivatives of htt$^{NT}$Q$_{37}$P$_{10}$K$_2$ peptides. (a) Aggregation kinetics analysis of htt$^{NT}$Q$_{37}$P$_{10}$K$_2$ peptides in PBSA at 37 °C by sedimentation analysis. WT (F17W) (black filled circles, 19 μM); S13D/S16D (red filled circles, 34 μM); S13p (blue open circles, 21 μM); S16p (red open circles, 20 μM); S13pS/S16pS (blue filled circles, 19.5 μM). (b–r) Electron micrographs of the aggregates of different htt$^{NT}$Q$_{37}$P$_{10}$K$_2$ peptides isolated at different time points. Aggregates of WT (F17W) at 47 h (b) and after 1 h (c); S13D/S16D after 100 h (d–g); S13pS/S16pS after 163 h (h–j); S13p (k and l) and S16p (m and n), both at 33 h; S13D/S16D aggregates at 1.5 h (o and p); and S13pS/S16pS aggregates at 2 h (q and r). The scale bar represents 50 nm.

of these two Ser residues to Asp might influence the folding and aggregation properties of such htt fragments, and how these changes might translate into the observed loss of aggregate accumulation in the mouse model, is the main subject of this report.

The nucleation mechanisms of polyQ amyloid formation have been analyzed in some detail, both in isolation[16,17] and in the context of the sequences flanking polyQ in the htt protein,[18–22] and both mechanisms are operative in polyQ-containing fragments of htt[23] (Fig. 2). Under most circumstances, the mechanism found in simple expanded polyQ repeat peptides, in which rare amyloid core nuclei are formed directly from within the monomer pool (Fig. 2, Path B), is largely outcompeted in htt fragment aggregation by an alternative mechanism featuring the key involvement of the htt$^{NT}$ sequence. In this much more efficient mechanism (Fig. 2, Path A), htt$^{NT}$ segments self-associate into α-helix-rich tetramers and higher oligomers, which serve to locally concentrate and/or align polyQ segments and facilitate the formation of amyloid nuclei. Interference with the formation of α-helical oligomers suppresses the normally dominant A pathway, allowing enhanced contributions from the B pathway.[23]

In this article, we show that these Ser-to-Asp mutations within htt$^{NT}$ influence aggregation rates, not by abrogating the α-helical oligomer pathway, but by decreasing its efficiency. We show that, in spite of solid-state NMR (ssNMR) data showing aggregate secondary structures similar to fragments with wild-type (WT) htt$^{NT}$, Ser-modified htt fragment aggregates exhibit substantial differences from WT in electron microscopy (EM) morphologies, in decreased stabilities toward dissociation, and in increased susceptibility of their htt$^{NT}$ segments to trypsin cleavage. These differences suggest several possible explanations for the dramatic phenotypes of the S13D/S16D tg mice. We also show that authentic phosphoryl-serine residues at positions 13 and 16 of polyQ-containing htt fragments exhibit aggregation properties similar to those of the corresponding Ser→Asp mutants, suggesting that this commonly used phosphomimetic mutation faithfully captures the aggregation-modifying effects of htt$^{NT}$ phosphorylation.

## Results

### Phosphorylation of htt$^{NT}$ serine residues impairs aggregation

To assess the importance of the negative charges introduced in the Ser-to-Asp mutations, as well as the ability of these mutations to mimic the effects of Ser phosphorylation, we obtained htt$^{NT}$Q$_{37}$P$_{10}$K$_2$ (F17W) peptides with one or both of the Ser residues at positions 13 and 16 phosphorylated (Fig. 1) and assessed their effects on overall aggregation kinetics (Fig. 3a). We found that, similar to the S13D/S16D mutant (red filled circles), the doubly phosphorylated S13pS/S16pS peptide (blue filled circles) exhibits substantially reduced aggregation compared to the WT peptide (black filled circles), with a greater rate suppression effect than that of the S13D/S16D mutant (Fig. 3a). Furthermore, overall aggregation rates of the single phosphoryl-Ser peptides S13pS (blue open circles) and S16pS (red open circles) are also slower than the WT rate (black filled circles) and similar to the S13D/S16D rate (red filled circles). Phosphorylation of these Ser residues also had effects similar to that of the S13D/S16D mutations[9] on aggregate morphologies in the EM. Similar to the S13D/S16D mutant peptides (Fig. 3d–g), the intermediate and final aggregates of the double (Fig. 3h–j) and single (Fig. 3k–n) phosphoryl-Ser peptides resemble the protofibrillar and oligomeric intermediates observed on incubation of polyQ-containing htt fragments with WT htt$^{NT}$ (Fig. 3c) and do not resemble mature fibrils (Fig. 3b). The results show that the Ser→Asp mutations are, in fact, good mimics of the disrupting effects of Ser phosphorylation on the ability of the htt$^{NT}$ sequence to stimulate polyQ aggregation, producing reduced aggregation kinetics and final morphologies that resemble those normally seen for reaction intermediates. This emphasizes the role of the introduced negative charges on these modified properties.

### Serine modifications affect oligomerization rates but not monomer conformations

One hypothesis for the molecular basis of HD posits that polyQ expansion leads to an alternative folded state within monomers that is responsible for pathology.[22] To probe for effects of htt$^{NT}$ serine modifications on the conformations of polyQ-containing htt fragments, we conducted solution spectroscopy experiments, working at low concentrations that disfavor helical bundle association and oligomerization[20] (Fig. 4a). We found no significant differences in the CD spectra of freshly disaggregated (Materials and Methods) solutions of the WT (black continuous line), S13D/S16D (red continuous line), and S13pS/S16pS (blue continuous line) versions of htt$^{NT}$Q$_{37}$P$_{10}$K$_2$ (Fig. 4a). Furthermore, using fluorescence resonance energy transfer (FRET) probes at positions −1 and 17 (Fig. 1) in the htt$^{NT}$Q$_{37}$P$_{10}$K$_2$ background, at 30 μM in phosphate-buffered saline (PBS) at pH 7.4, we found no difference in the estimates of average −1 to 17 distance for the WT (31.9±0.1 Å) and S13D/S16D (31.8±0.3 Å) peptides. Thus, there is no indication from these low-resolution methods that these Ser modifications within htt$^{NT}$ influence monomer conformation.

In contrast, we found that negatively charged residues at positions 13 and 16 impart a thermodynamic barrier onto the first step in the amyloid formation mechanism (Fig. 2, Path A), oligomer formation. While the WT htt$^{NT}$ sequence (black filled circles) undergoes concentration-dependent, reversible assembly into α-helix-rich oligomers with a midpoint of about 0.5 mM, the S13D/S16D mutant (red filled diamonds) exhibits a much less cooperative assembly curve with a midpoint of about 0.9 mM (Fig. 4b). Furthermore, in peptides of the sequence htt$^{NT}Q_8K_2$ (Fig. 1), a background that supports very slow htt$^{NT}$-mediated nucleation of polyQ amyloid formation,[20] the S13D/S16D mutation (red filled diamonds) greatly diminishes the time-dependent formation of sedimentable oligomeric intermediates compared to WT htt$^{NT}$ (black filled circles) (Fig. 4c).

At first glance, the ability of negatively charged groups at positions 13 and 16 to reduce the formation of htt$^{NT}$ α-helix-rich oligomers is somewhat puzzling. The helical wheel diagram of htt$^{NT}$[12,13] (Fig. 4b, inset) shows a strong amphipathic nature, and recent results suggest that the hydrophobic face of this helix plays a major role in oligomer stabilization (R.M. and R.W., unpublished results). However, Ser13 and Ser16 are on the *hydrophilic* face of the α-helix, which is predicted to be solvent exposed and therefore not expected to play a major role in oligomer formation. One possible explanation of the surprising ability of these mutations to suppress α-helical oligomer formation is that this hydrophilic face may be involved in packing of α-helical tetramers into higher-order oligomers that might be required for stabilizing oligomers and ultimately for amyloid nucleation. Alternatively, charge repulsion between positions 13 and 16 in the neighboring turns of the helix might destabilize α-helix formation and hence affect overall oligomer stability.

For both WT and S13D/S16D htt$^{NT}Q_8K_2$ sequences, the oligomers formed are α-helix rich by Fourier transform infrared (FTIR) spectroscopy (Fig. 4d). In spite of the much less favorable and slower formation of α-helix-rich aggregates, the S13D/S16D htt$^{NT}Q_8K_2$ peptide is able to undergo nucleation of β-rich, amyloid-like structure with similar kinetics to WT htt$^{NT}$. This is shown by the previously described[19,20] transition, within the

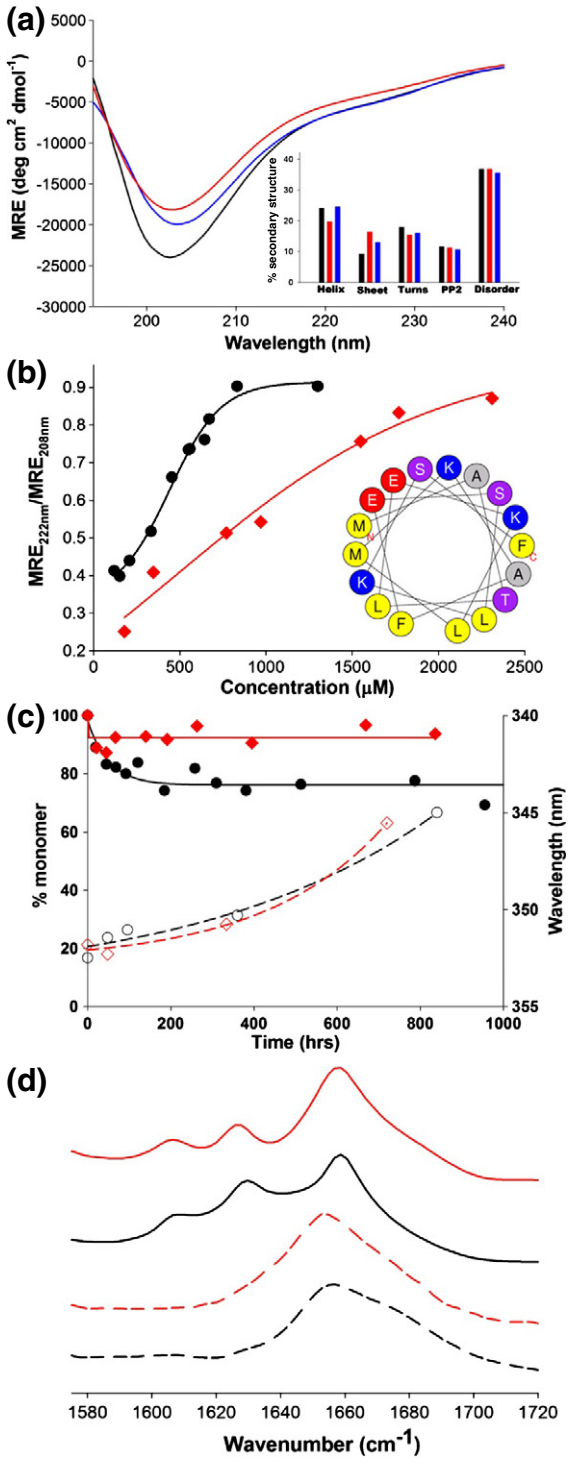


**Fig. 4.** Structural consequences of Ser modification during aggregation. (a) CD spectra of htt$^{NT}Q_{37}P_{10}K_2$ peptides [WT (black), S13D/S16D (red), and S13pS/S16pS (blue)] at ~35 μM in 10 mM Tris–HCl, pH 7.4; inset, secondary-structure composition estimates from the CD curves (Materials and Methods). (b) Concentration dependence of α-helix structure in isolated htt$^{NT}$ peptides of WT (black filled circles) and S13D/S16D (red filled diamonds) sequence; inset, helical wheel analysis of htt$^{NT}$, with alanine residues in gray, hydrophobic amino acids in yellow, acidic residues in red, basic residues in blue, and neutral hydrophilic residues in violet. (c) Aggregation kinetics of htt$^{NT}Q_8K_2$ peptides by sedimentation [WT (black filled circles), S13D/S16D (red filled diamonds)] and by Trp fluorescence of isolated aggregates [WT (black open circles), S13D/S16D (red open diamonds)]. (d) FTIR spectra of the aggregates of the htt$^{NT}Q_8K_2$ peptides isolated at different times: WT at 48 h (black broken line) and 840 h (black continuous line); S13D/S16D at 48 h (red broken line) and 720 h (red continuous line).

aggregate pool, of the Trp at position 17 from a solvent-exposed ($\lambda_{emm}$ ~351–353 nm) to a solvent-excluded ($\lambda_{emm}$ ~345 nm) environment [Fig. 4c, compare WT (black open circles) to S13D/S16D (red open diamonds)] and in the development of FTIR bands, including β-sheet (1625–1630 $cm^{-1}$), characteristic of a polyQ amyloid structure [Fig. 4d, compare WT (black continuous line) to S13D/S16D (red continuous line)].

### Serine modifications and polyQ amyloid nucleation and elongation

Collection of time-dependent spectroscopic changes, as described above, is a useful approach for gauging aggregate structure in short polyQ-containing htt fragments but is problematic for rapidly aggregating, long polyQ versions due to the difficulty in collecting useful amounts of early pre-nucleation aggregates. We therefore used other probes to assess the mechanistic impact of serine modifications in fragments with disease-relevant repeat lengths. The concentration dependence of initial aggregation rate has proved a good gauge of nucleation mechanism in this system. Thus, peptides undergoing nucleation without help from the $htt^{NT}$ flanking sequence (i.e., Fig. 2, Path B) typically exhibit log–log slopes in the range of 3 or higher,[16–18,21,24,25] while peptides undergoing nucleation facilitated by a flanking $htt^{NT}$ sequence (i.e., Fig. 2, Path A) exhibit slopes in the range of ~1.[19,21] We found that the slope of an analogous log–log plot for the S13D/S16D mutant of $htt^{NT}Q_{37}P_{10}K_2$ is ~1.3 (Fig. 5a), consistent with a nucleation mechanism that is predominantly $htt^{NT}$ mediated (Fig. 2, Path A).

Another useful probe is the response of the aggregation reaction to mechanism-specific aggregation inhibitors. Recently, we reported that peptides consisting of $htt^{NT}$ with few if any attached Gln residues are able to transiently inhibit $htt^{NT}$-mediated amyloid nucleation by co-assembling with polyQ-containing htt fragments into a mixed α-helix-rich oligomer, thereby reducing the local polyQ concentration in the oligomers and hence the amyloid nucleation efficiency.[21] We find that, in fact, the S13D/S16D mutant of $htt^{NT}Q_{37}P_{10}K_2$ responds to inhibition by an $htt^{NT}Q_3$ peptide with a similar retardation of aggregation onset as the WT peptide (Fig. 5b). Thus, consistent with the slope of the log–log plot (Fig. 5a), sensitivity to $htt^{NT}$ inhibition indicates a major role for the $htt^{NT}$ domain in facilitating the aggregation of the S13D/S16D mutant. We also previously described inhibitors such as $PGQ_9P^{1,2,3}K_8$ (Fig. 1). Such peptides inhibit the elongation of amyloid-like aggregates of simple polyQ and, because of the importance of elongation in the nucleation process, also suppress spontaneous amyloid formation by simple polyQ peptides.[22,26] Presumably because the nucleation of $htt^{NT}$ containing polyQ peptides is dominated by $htt^{NT}$-mediated oligomer formation, we find that the polyQ amyloid elongation inhibitor $PGQ_9P^{1,2,3}K_8$ gives no detectable inhibition

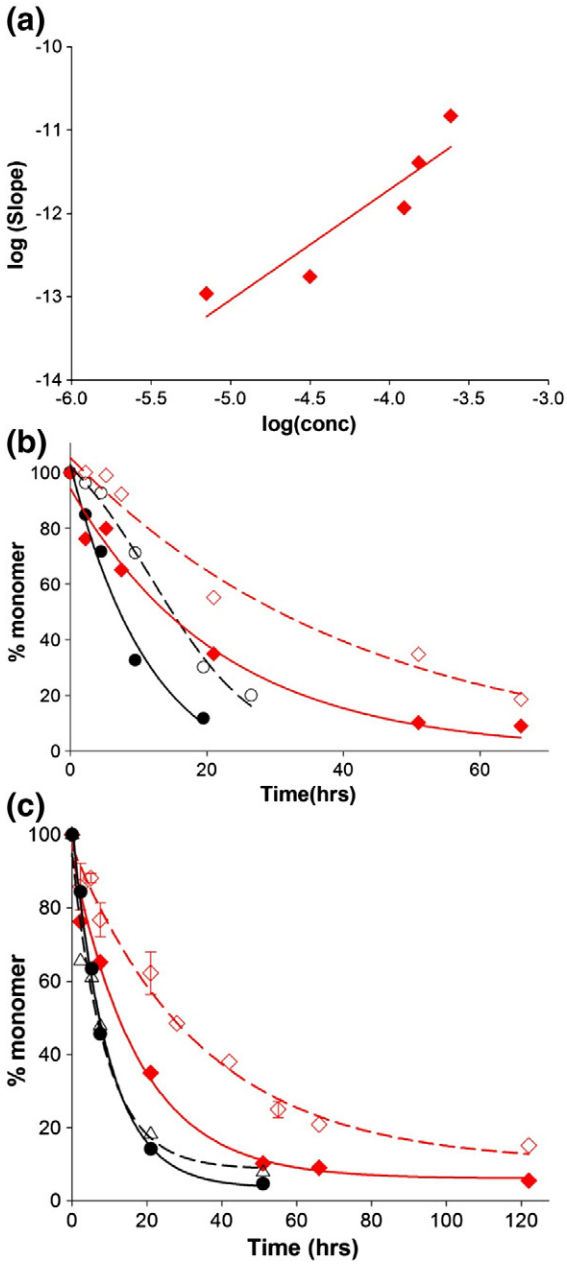


**Fig. 5.** Aggregation kinetics consequences of S13D/S16D mutation in $htt^{NT}Q_{37}P_{10}K_2$. (a) Concentration dependence of initial phase of the aggregation reaction. (b) Inhibition of aggregation by 1:1 ratio of $htt^{NT}Q_3$ to peptide. WT alone (black filled circles, 50 μM) and with inhibitor (black open circles, 48 μM); S13D/S16D alone (red filled diamonds, 43 μM) and with inhibitor (red open diamonds, 68 μM). (c) Inhibition of aggregation by ~5-fold excess of elongation inhibitor $PGQ_9P^{1,2,3}K_8$ compared to peptide. WT alone (black filled circles, 22 μM) and with inhibitor (black open circles, 26 μM); S13D/S16D alone (red filled diamonds, 43 μM) and with inhibitor (red open diamonds, 34 μM).

of spontaneous aggregation of WT htt$^{NT}Q_{37}P_{10}K_2$ (Fig. 5c). Interestingly, however, this inhibitor does inhibit spontaneous aggregation of the S13D/S16D mutant (Fig. 5c). Further studies will be required to elucidate the mechanistic basis of this effect. However, the different responses of the WT and S13D/S16D peptides to the $PGQ_9P^{1,2,3}K_8$ inhibitor provides further evidence for the mechanistic impact of the negatively charged residues in htt$^{NT}$ on aggregation.

Overall, these mechanistic probes support the view that Ser modifications in htt$^{NT}$ do not alter the fundamental, htt$^{NT}$-mediated nucleation mechanism of htt N-terminal fragments (Fig. 2, Path A), but rather influence the efficiency of this mechanism. The reductions in overall aggregation rate previously reported for the S13D/S16D mutant,[9] and reported here for the phosphoryl-Ser peptides (Fig. 3a), appear to be primarily due to less favorable formation of the α-helix-rich oligomeric intermediates that are the springboard for amyloid nucleation (Fig. 2, Path A).

## Serine modifications and aggregate structure and stability

Previously, we reported magic angle spinning (MAS) ssNMR data on mature amyloid fibrils of htt$^{NT}Q_{30}P_{10}K_2$ peptides that confirmed the expected β-structure in many of the polyQ Gln residues while surprisingly showing that residues 4–11 of the htt$^{NT}$ reside in stable α-helix.[27] We acquired the corresponding S13D/S16D peptide containing U-$^{13}$C, $^{15}$N-labeling of particular residues within the α-helix, the polyQ segment, and the intervening linker region, and then prepared mature fibrils and collected MAS ssNMR data. We used chemical shift indexing relative to data on proteins of known structure to infer secondary structure at the labeled positions.[28] The results (Fig. 6) show that the labeled sites in S13D/S16D fibrils have chemical shifts, and thus structures, that are remarkably similar to that of the WT htt$^{NT}$ peptide. Thus, the Lys6 and Ala10 residues of S13D/S16D exhibit the same kind of strong α-helical signal as found in the WT peptide aggregates. For Leu14, despite a slightly increased indication of α-helicity for the C$^{\alpha}$ shift alone, the overall chemical shift pattern for this residue in the S13D/S16D protein, as in the WT protein, is not indicative of a well-defined secondary structure. Note that electrostatic or structural effects due to the mutation of the neighboring S13 may affect the observed chemical shifts and in part explain these chemical shift changes. Finally, as in the previously reported aggregates with WT htt$^{NT}$, a specifically labeled Gln18 is found in two chemically distinct environments, both of which are β-conformations. The S13D/S16D aggregates exhibit an essentially identical split β profile. Thus, in spite of significant differences in EM morphology, the S13D/S16D peptide aggregates are indistinguishable at the level of secondary structure from the WT htt$^{NT}$ aggregates, at least at the labeled residues. This is consistent with the above kinetics data suggesting an unchanged aggregation mechanism compared with the WT sequence.

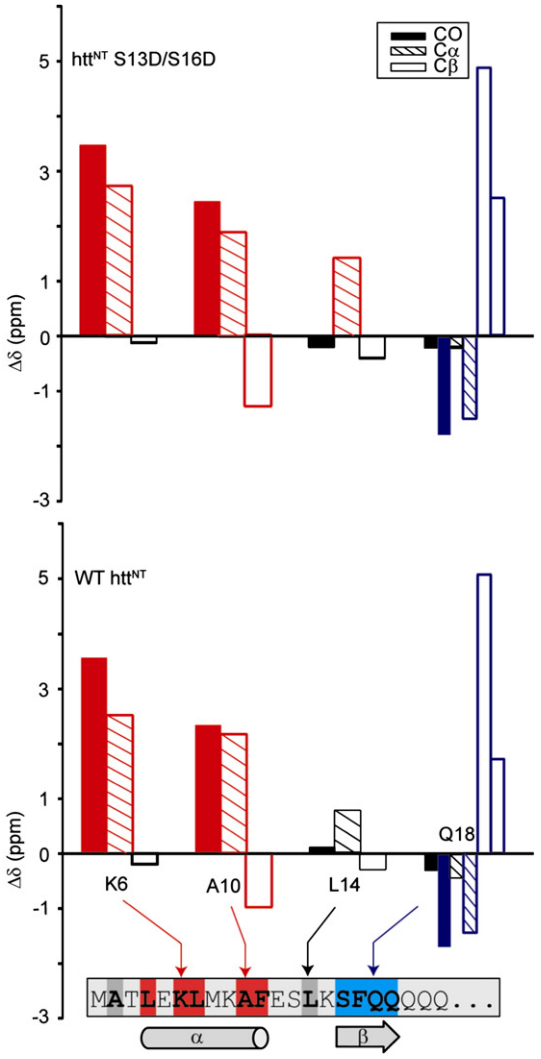


**Fig. 6.** Structural consequences of Ser modification in mature htt$^{NT}Q_{30}P_{10}K_2$ aggregates. Graphical representation of the $^{13}$C secondary chemical shifts (Δδ) obtained for indicated labeled residues, based on MAS ssNMR on mature aggregates from S13D/S16D (top) and WT (bottom) peptides. Δδ values were determined as differences from random-coil chemical shifts for CO, C$^{\alpha}$, and C$^{\beta}$ sites. The local secondary structure inferred from those values is shown. Red bars represent α-helicity, whereas blue bars indicate β-sheet structure. Black bars indicate a lack of defined secondary structure. Split bars for Gln18 indicate two sets of observed NMR signals associated with two conformations, both β.

To complement these ssNMR results, we performed other tests probing for changes in aggregate

structure and stability introduced by serine modifications. We exposed final aggregates of various $htt^{NT}Q_{37}P_{10}K_2$ peptides, after fractionation from any non-aggregated monomers by centrifugation, to limited trypsin proteolysis—a sensitive, if low-resolution, probe of amyloid structure,[29] and analyzed the results by LC-MS. We found that mature WT aggregates are relatively stable to cleavage within the $htt^{NT}$ segment, with only about 10% of the peptides being cleaved, all at Lys6 (Fig. 7a, black bars). In contrast, about 30% of the peptides in S13D/S16D aggregates (red bars) and nearly 50% of the peptides in S13pS/S16pS aggregates (blue bars) are cleaved by trypsin exposure under the same conditions. Interestingly, the single phosphoryl-Ser mutants, S13pS and S16pS, are both about 30% cleaved, the same level as the S13D/S16D aggregates; thus, the sensitivity of these modified Ser aggregates to trypsin cleavage rank very similarly to their relative formation rates in the kinetics analysis (Fig. 3a). We also examined the trypsin cleavage sensitivities of the aggregates of some of these peptides isolated relatively early (30–35% completion) in the aggregation reactions. We observed trypsin susceptibilities in these early/intermediate aggregates very similar to those in the mature aggregates (Fig. 7a).

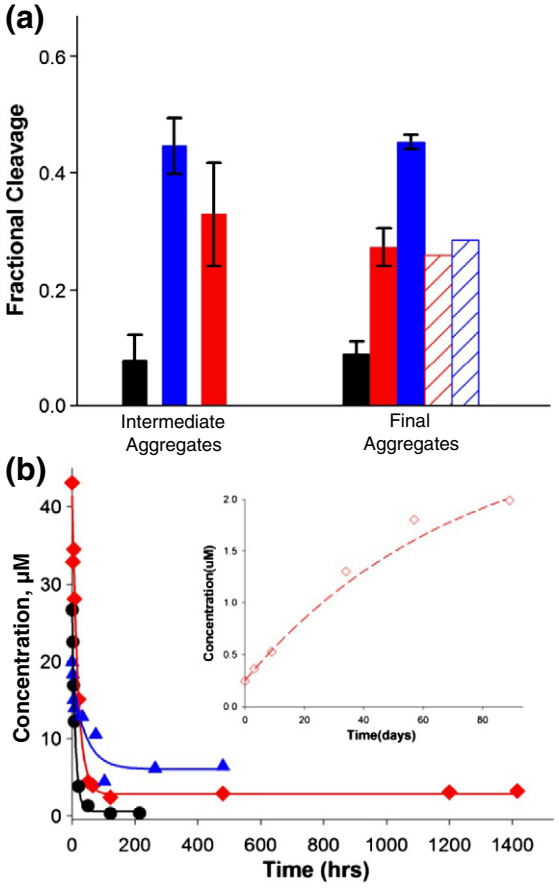


**Fig. 7.** Structural consequences of Ser modification in mature $htt^{NT}Q_{37}P_{10}K_2$ aggregates. (a) Fraction of molecules cleaved within $htt^{NT}$ after exposure to trypsin in various mature aggregates (WT, black bars; S13pS/S16pS, blue bars; S13D/S16D, red bars; S13pS, red hatched bar; S16pS, blue hatched bar). (b) Sedimentation assays of aggregation kinetics and plateau levels of monomer for WT (black filled circles), S13D/S16D (red filled diamonds), and S13pS/S16pS (blue filled triangles) peptides in PBS at 37 °C. Inset: Dissociation of S13D/S16D aggregates in PBS at 37 °C by sedimentation assay.

In addition to a greater amount of cleaved material, we also observed "deeper" cleavages in the digests of fibrils from the $htt^{NT}$ mutated peptides. Thus, while the small amount of cleavage of WT fibrils was all at Lys6, cleavage of fibrils from mutated $htt^{NT}$ peptides occurred at both Lys6 and Lys9. About equal amounts of fragments from cleavage at positions 6 and 9 were obtained on digestion of the S13D/S16D mutant fibrils, while the position 9 fragment predominated in the digest of the S13pS/S16pS fibrils.

The changes in aggregate stabilities suggested by the limited proteolysis experiments are consistent with a robust measure of global stability,[30,31] the concentration of monomeric peptide remaining when the aggregation reaction reaches equilibrium. This residual monomer concentration, which typically can be reached in both the aggregate association and dissociation directions,[17,30] is essentially the critical concentration, or $C_r$, for the polymerization reaction and hence is linked to the thermodynamic favorability of aggregate elongation.[30,31] We found a surprisingly dramatic effect of the Ser modifications within $htt^{NT}$ on this measure of aggregate stability. We found that the aggregation reaction of WT $htt^{NT}Q_{37}P_{10}K_2$ reaches equilibrium, with a $C_r$ in the 0.3 μM range, after about 50 h, with no further change up to 200 h (Fig. 7b, black filled circles). In comparison, the corresponding S13D/S16D peptide aggregation reaction reaches a plateau in monomer concentration in the 2.5–3.0 μM range after about 100 h, with no further change out to 1400 h (Fig. 7b, red filled diamonds). A similar monomer concentration of 2 μM is reached when S13D/S16D aggregates are diluted and given the opportunity to dissociate toward equilibrium (Fig. 7b, inset), showing the robustness of the measurement as a quantity associated with a dynamic equilibrium. The S13pS/S16pS peptide requires about 200 h to reach equilibrium where it indicates a $C_r$ value in the 4.5–6.0 μM range (Fig. 7b, blue filled triangles). Based on these values, we calculated the aggregation destabilization ($\Delta\Delta G_{ag}$)[31] attributable to the negative charges introduced at the Ser residues to be ~1.3–1.4 kcal/mol for the S13D/S16D mutation and ~1.7–1.8 kcal/mol for the S13pS/S16pS peptide. Since the $C_r$ value is the concentration below which aggregation cannot occur, these $C_r$ values may have important practical consequences for cellular aggregate accumulation.

## Discussion

Protein phosphorylation and dephosphorylation play an enormous role in cell regulation and cell pathway dysfunction linked to disease.[32] Phosphorylation of the protein huntingtin,[33,34] especially at Ser421[35] and within the N-terminal htt$^{NT}$ sequence,[14,15,36,37] has been implicated in controlling a variety of this protein's cellular activities. Phosphorylation at serines 13 and 16 has been implicated in enhanced degradation of htt by the proteasome in cell models,[14] in suppressed accumulation of htt aggregates in a mouse model,[9] and in enhanced htt transport into the nucleus.[14,15,37] The dramatic effects on aggregate accumulation and HD phenotype of the phosphomimetic S13D and S16D mutations in the BACHD mouse model suggest that persistent phosphorylation of these residues in the cell could play an equally strong role in abrogating the effects of an expanded polyQ sequence in huntingtin. The possible impact of partial and/or transient phosphorylation is more difficult to assess from the *in vitro* aggregation results.

Regardless of the implications for a strong role for phosphorylation, the dramatic effects of the S13D/S16D mutations in mice offer an opportunity to explore elements of the HD disease mechanism. That is, it is clear that mutation of these Ser residues to Asp, at only two positions out of over 3000 residues in full-length htt, dramatically neutralizes the aggregation effects of a $Q_{97}$ repeat in this system.[9] We therefore focused our efforts on understanding how this double mutation influences various aspects of htt aggregation. Our previous results showed that replacement of Ser13 and Ser16 with Asp significantly reduced the rate of amyloid formation in an htt exon1-like peptide and dramatically changed the morphology of the aggregates.[9] In that paper, we speculated that diminution of the aggregation rate could affect the accumulation of aggregates by allowing the cellular mechanisms of aggregate eradication[38,39] to better keep up with aggregation. Here, we describe the underlying molecular basis of this diminution in aggregation rate, as well as some potentially equally important differences conferred on the product fibrils. We also show that the Ser-to-Asp mutation is in fact a reasonable approximation for the effect of stable, 100% phosphorylation of these two Ser residues on amyloid formation rates and amyloid structure.

In principle, there are a number of mechanistic steps that might be targeted by htt$^{NT}$ sequence changes to explain observed aggregation rate reductions. These include control of monomer conformation, oligomer formation, amyloid nucleation and amyloid elongation. Our studies show that only one of these mechanisms is consistent with the data. We found that the S13D/S16D mutation does not appreciably affect the ensemble monomeric conformation of the htt$^{NT}Q_{37}P_{10}K_2$ peptides based on CD (Fig. 4a) and FRET (Results). (In contrast, Truant *et al.* described CD experiments showing significant reductions of α-helix in htt$^{NT}$ peptides modified on the Ser residues, which they interpreted as evidence for altered monomer conformations.[15] The different results may be due to sample disaggregation procedures, peptide sequence background used, or peptide concentrations used.) The htt$^{NT}$ Ser modifications also do not appear to change the fundamental amyloid nucleation mechanism, which is equally dependent, for both WT and S13D/S16D peptides, on the initial formation of htt$^{NT}$-mediated α-helix-rich oligomers (Fig. 5a and b). Likewise, by using short polyQ versions of exon1-like peptides, we show that the S13D/S16D mutations have no great effect on the amyloid nucleation and elongation reactions once α-helix-rich oligomers have formed (Fig. 4c and d). In contrast to these negative findings, we observed that htt$^{NT}$ segments containing the S13D/S16D mutations are thermodynamically impaired in their assembly into α-helix-rich oligomers (Fig. 4b and c). Thus, the most likely source of the observed diminished spontaneous aggregation rates is a reduced ability to form the α-helix-rich tetramers and higher aggregates that serve as the species within which polyQ amyloid structure is nucleated[19,20,22] (Fig. 2).

These results for Ser-to-Asp mutations within htt$^{NT}$ on the solution structure and reactions of exon1-like monomers are replicated in peptides in which one or both of the Ser residues are phosphorylated. Thus, the approximate secondary structural distribution within the monomer ensemble of the S13pS/S16pS peptide is indistinguishable from both the WT htt$^{NT}$ sequence and the S13D/S16D double mutant (Fig. 4a). Likewise, aggregation of htt$^{NT}Q_{37}P_{10}K_2$ peptides in which one or both of the htt$^{NT}$ Ser residues are phosphorylated is slowed dramatically (Fig. 3a); in fact, the S13pS/S16pS peptide aggregates substantially less rapidly than the S13D/S16D peptide, presumably due to the more highly charged nature of the phosphoryl groups compared with carboxylate groups.

Thus, we obtained consistent data suggesting that the homogeneous, stable phosphorylation of Ser13 and Ser16, or their replacement with Asp residues, is expected to lead to slower kinetics of formation of amyloid fibrils due to the reduced stability of the transient oligomers that are required for amyloid nucleation. By slowing amyloid formation rates, these sequence alterations might allow cellular processes to better manage aggregate formation and therefore suppress aggregate accumulation. It also seemed possible, however, that alterations in the structures and properties of the product fibrils once formed might contribute to the tg mouse phenotype. We therefore compared the aggregate structure and properties of WT peptides and peptides with modifications at residues 13 and 16.

We examined the final amyloid-like aggregates grown from the S13D/S16D htt$^{NT}$Q$_{37}$P$_{10}$K$_2$ peptide by ssNMR and found that, just as in WT fibrils,[27] residues 4–11 exist in α-helix, residue 14 is in irregular structure, and Gln18 is in β-sheet (Fig. 6). This result confirms the importance of α-helix formation by htt$^{NT}$ in the aggregation mechanism as well as showing no major difference in residue specific secondary structural preferences between WT and mutant aggregates. In spite of these similar secondary structural profiles, however, further examination showed significant differences in structure and properties between WT and htt$^{NT}$-mutated exon1 fibrils.

For example, electron micrographs clearly show a difference in aggregate morphology[9] (Fig. 3). Thus, while WT htt$^{NT}$ exon1 fibril preparations are essentially homogeneous, exhibiting long, single fibrils with rough edges (Fig. 3b), final aggregates from peptides containing either Ser-to-Asp mutations or phosphoryl-Ser in the htt$^{NT}$ segment are a mixture of morphologies including large bundles of thin filaments (Fig. 3d and h), amorphous aggregates (Fig. 3e and j), and short, protofibril-like structures (Fig. 3f, g, and i) reminiscent of an early reaction intermediate in the WT reaction (Fig. 3c).

Additionally, the final aggregates from htt$^{NT}$Q$_{37}$P$_{10}$K$_2$ peptides containing either S13D/S16D or S13pS/S16pS replacements are dramatically more susceptible to trypsin (Fig. 7a). Thus, WT fibrils subjected to limited trypsin digestion suffer less than 10% cleavage, all of which occurs at residue 6, the most distal Lys residue from the polyQ amyloid core. In contrast, S13D/S16D final aggregates under the same conditions are cleaved in about 30% of the constituent molecules, with a distribution of about equal portions of cleavage at Lys6 and Lys 9. Finally, final aggregates of the S13pS/S16pS peptide are cleaved within htt$^{NT}$ in almost 50% of the constituent peptides, and most of the cleavages occur at Lys9 nearer the polyQ amyloid core. This suggests significantly greater access by trypsin, and therefore perhaps other enzymes, to the htt$^{NT}$ segments within the aggregates containing negative charges at the normal Ser positions. This suggests that these aggregates may be more susceptible to *in vivo* proteolysis than WT aggregates. In addition, this indication of different degrees of steric access might be relevant to the known ability of htt fragments to be ubiquitinylated at the N-terminus[11,14] and to suspicions that ubiquitin-targeted proteasomal degradation plays a large role in the cell's ability to remove htt aggregates.[1] If ubiquitinylating enzymes have greater access to the Lys residues that are the targets of ubiquitin modification in the aggregates of phosphomimetic and phosphorylated peptides, compared to WT, this might suggest a greater ability of the ubiquitin system to target mutant aggregates for proteasome degradation, consistent with the lack of inclusion accumulation in the S13D/S16D BACHD mice.

Finally, the measured $C_r$ values for various exon1 fragments suggest that mutations introducing negative charges at positions 13 and 16 of htt$^{NT}$ abrogate the positive contribution of htt$^{NT}$ to fibril stability. Thus, we previously reported $C_r$ values for K$_2$Q$_{36}$P$_{10}$K$_2$ and K$_2$Q$_{40}$P$_{10}$K$_2$ peptide fibrils in the 2–4 μM range under the same growth conditions used in the experiments described here.[18] The covalent attachment of htt$^{NT}$ to such molecules, in the WT peptide htt$^{NT}$Q$_{37}$P$_{10}$K$_2$, reduces the $C_r$ to the 0.3 μM range (Results). However, the $C_r$ of a similar molecule containing negative charges at positions 13 and 16 reduces stability to $C_r$ values of ~2.5 μM for the S13D/S16D sequence and ~5 μM for the S13pS/S16pS sequence (Results). Thus, introduction of these negative charges destabilizes htt exon1-like fibrils to a range essentially identical with that of fibrils from similar sequences lacking htt$^{NT}$ entirely. The implications for exon1 fibril structure are not entirely clear. Part of the stabilization contributed by htt$^{NT}$ could derive from the involvement of the aromatic residue at position 17 in β-structure,[27] and part could derive from helix–helix interactions. In any case, it is clear that the negative residues at positions 13 and 16 somehow compromise these htt$^{NT}$ contributions and that this may have consequences for aggregate stability within the cell. These results are consistent with several recent model peptide studies demonstrating a general ability of phosphorylation to modify the kinetics and product structure of amyloid formation.[40–42]

Together, the results of analysis of aggregate structures and properties suggest that placing negative charges at positions 13 and 16 decreases aggregate thermodynamic stability (both in the early htt$^{NT}$-mediated oligomers and the mature fibrils) as well as increases the accessibility of the htt$^{NT}$ terminus to enzyme modification. Although these results may appear to be inconsistent with the ssNMR results showing approximately equivalent secondary structures for the WT and S13D/S16D aggregates, we suggest that the results merely reflect the different methods' complementary insights into fibril structure, dynamics, and stability. Thus, the ssNMR experiments are exquisitely sensitive to the local structure of the immobilized material (i.e., the atomic structure of the protofilaments) but lack direct information on nonlocal interactions such as changes in morphology as seen by EM (i.e., supramolecular assembly of smaller units into fibrils). The ssNMR experiments also detect the overall signals of the bulk sample, in particular the most rigid parts of the molecule (see also Ref. 27). These points are brought out by the hypothetical model shown in Fig. 8.

The Fig. 8 model (as well as the Fig. 2f model) proposes that the htt$^{NT}$ segments of peptides within a filament interact with and stabilize each other. It also proposes that the htt$^{NT}$ segments may be largely responsible for the filament–filament interactions required to build up the thicker fibrils seen for

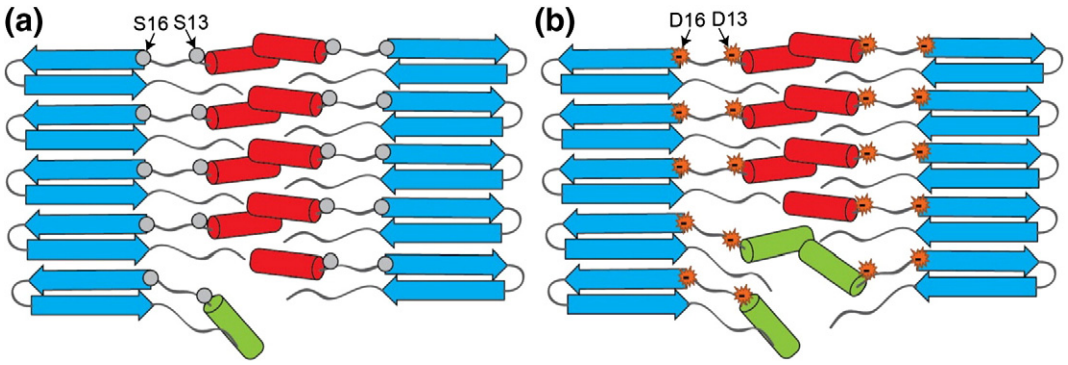


**Fig. 8.** A model for the htt exon1-like fibril structure, integrating observations from ssNMR, EM, and trypsin cleavage. In the figures, polyQ β-sheets are in blue, more rigid htt$^{NT}$ α-helices are in red, and more mobile htt$^{NT}$ α-helices are in green. Positions 13 and 16 are in a segment lacking secondary structure.[27] The figure shows how increased mobility (green helices) caused by charge repulsion (b) leads to greater exposure of htt$^{NT}$ sequences to trypsin access compared to more stably packed WT htt$^{NT}$ (a). In both WT and mutated htt$^{NT}$, the bulk of the htt$^{NT}$ helices (red) remain stably involved in structure and detectable by MAS ssNMR.

WT exon1-like aggregates (Fig. 3b). This model is similar to a recently proposed model for the role of htt$^{NT}$ in fibril structure based on EPR data.[43] Since the addition of negative charges in htt$^{NT}$ occurs in the "linker" part of the peptide between the β-sheet and α-helix in the mature fibrils,[27] it will not necessarily disturb the α-helix in residues 4–11 observed by ssNMR in the final aggregates. At the same time, charge repulsion could introduce destabilization that manifests in the EM, $C_r$, and trypsin data presented. Thus, repulsion could interfere with fibril assembly resulting in the accumulation of filaments (compare Fig. 3b to Fig. 3d and h). Second, charge repulsion could reduce the htt$^{NT}$ contribution to fibril stability, as observed in the $C_r$ values (Fig. 7b). Third, charge repulsion could lead to more dynamic unfolding–refolding of the α-helices, at least at certain locations such as fibril ends, thus increasing the sensitivity of htt$^{NT}$ to trypsin (Fig. 7a). The model in Fig. 8 may account for why only a subset of the htt$^{NT}$ segments (the green helices in the figure) are trypsin sensitive, being in an environment (fibril termini in the schematic) that is particularly sensitive to charge repulsion effects. The model also suggests that the bulk of the htt$^{NT}$ segments in both WT and S13D/S16D fibrils are expected to be found in α-helix in the MAS ssNMR experiments.

Taken together, our studies on the S13D/S16D peptide indicate a number of possible biophysical explanations for the absence of inclusions in the tg mice carrying these mutations. First, the mutations decrease the tendency of the disordered htt$^{NT}$ sequence to engage in α-helical tetramer formation, reducing the steady-state concentration of helical oligomers and consequently the rate of amyloid nucleation and growth. Second, the mature aggregates produced are less thermodynamically stable, to the extent that there is less of a driving force for their formation in the cell. Third, the htt$^{NT}$ segment in these aggregates is more accessible to trypsin, and perhaps to other enzymes such as ubiquitinylating enzymes, potentially providing a biophysical mechanism leading to increased proteasomal degradation.

Mutations of Ser or Thr residues to Asp or Glu residues have long been successfully used as ribosomally programmable mimics of phosphorylated residues, in spite of the dramatically different sizes and p$K_a$ values of carboxylic acid and phosphoric acid moieties. Our results show that Asp mutations can also be reasonable mimics of the effects of phosphorylation of Ser residues on protein aggregate formation rates and properties. Many substrates for phosphorylation are intrinsically disordered proteins, and the mechanisms by which phosphorylation imparts cellular effects have a strong protein folding component.[44] Our results suggest one feasible pathway by which protein phosphorylation might generally impact protein misfolding and aggregation, by directly modulating the long-term viability of disordered proteins in the cell. More specifically, the data provide a consistent mechanism to explain the lack of aggregate accumulation, and potentially the lack of toxicity, of S13D/S16D htt in a mouse model of HD. Since these Ser modifications suppress amyloid formation by first suppressing oligomer formation, the results suggest that α-helix-rich oligomers, while not visible in the mouse brain, also remain among the list of suspects as possible toxic agents in HD.

## Materials and Methods

### Materials

Water (HPLC grade), acetonitrile (99.8% HPLC grade), HFIP (99.5%, spectrophotometric grade), and formic acid were from Acros Organics; trifluoroacetic acid (99.5%

purity) was from Pierce; and thioflavin T was from Sigma. Chemically synthesized peptides (Fig. 1) were obtained either from the Keck Biotechnology Center at Yale University† or from GenScript, Inc. and purified on an Agilent Zorbax C3 reverse-phase HPLC column before use. Most peptides contained a conservative Phe→Trp replacement at position 17 previously shown to have little effect on aggregation rates.[19]

### General methods

All peptides were rigorously disaggregated as previously described.[45,46] Peptide concentrations were determined by analytical HPLC based on standard curves[45] from stock solutions of purified peptides calibrated as previously described.[20] For Trp fluorescence, FTIR analysis, and trypsin digestion studies, aggregates were isolated from reaction mixtures at specified time points by centrifugation at 21,000*g* for 45 min and the pellets were washed three times by resuspension and resedimentation with PBS to remove traces of trifluoroacetic acid and the other solutes. Aggregate concentrations were determined directly[45] or estimated from the measured monomer concentrations of aggregation reactions. A sedimentation/analytical HPLC assay[45] was used to determine aggregation and aggregate dissociation[17,30] kinetics. Trypsin-limited proteolysis was performed as previously described[46] on aggregates isolated as described above using 12 h incubation at a 1:25 weight ratio of trypsin to aggregate in 50 mM Tris–HCl, pH 7.0, at 37 °C. Transmission electron microscopy was on uranyl acetate negative-stained samples as previously described.[17,46]

### Spectroscopic methods

Far-UV CD measurements were performed on a JASCO J-810 spectropolarimeter using a 0.1-mm or 1-mm path length cuvette. Samples for CD measurement were prepared as previously described.[46] CD spectra were analyzed using the CONTINLL program[47] from the CDPro package‡ in which the SP37A reference set (ibasis 5) was used to estimate the amount of secondary structure. For FTIR analysis, aggregates isolated from 1- to 2-mM reactions were analyzed on an ABB Bomem FTIR instrument. Spectra were obtained by averaging a total of 400 scans collected at room temperature with 4 $cm^{-1}$ resolution. Residual buffer absorption was subtracted and spectral components were identified from second-derivative minima using PROTA software (Biotools, Inc.). Tryptophan fluorescence measurements on aggregates were as previously described.[46] Methods for acquiring ssNMR data have been previously described.[27]

### Limited trypsin digestion

For quantification of trypsin digestion, aggregates were isolated by centrifugation and resuspended in buffer, and the aggregate concentration was determined by dissolving an aliquot in formic acid and quantifying by the HPLC assay. These aggregates were then incubated at concentrations of 25–50 μg/ml in 50 mM Tris–HCl, pH 7.0, for 12–16 h at 37 °C in the presence of trypsin at a 1:25 weight ratio of trypsin (SEQUENZ-Trypsin, Worthington Biochemical Corp.) to protein. At the end of the incubation, the aggregates were isolated by sedimentation, washed twice with 50 mM Tris–HCl, pH 7, buffer, and then dissolved in formic acid and injected onto LC-MS (Agilent 1100 electrospray). Unique elution positions were obtained for full-length peptide and for peptides cleaved at positions 6 and 9. Structures of these peptides were confirmed by MS (see Supplemental Table 1). To quantify digestion, we integrated the A215 peaks to determine the relative amounts of intact and nicked $htt^{NT}Q_{37}P10K_2$. The ratio of the area of the fragment(s) to the total [i.e., intact plus fragment(s)] peptide area was then used to determine the fraction of the total aggregate that was cleaved.

### FRET measurements

FRET efficiencies were calculated based on a ratiometric approach on the basis of measured donor ($I_D$) and acceptor ($I_A$) fluorescence intensities from the protein tagged with a pair of FRET fluorophores (see Supplemental Methods).

Supplementary data to this article can be found online at http://dx.doi.org/10.1016/j.jmb.2012.09.011

## Acknowledgements

We thank Drs. James Conway and Alexander Makhov for access to the Structural Biology Department cryo-EM facility and acknowledge funding support from the National Institutes of Health (grant R01 AG019322 to R.W. and P.v.d.W.).

*Received 1 May 2012;*
*Received in revised form 1 September 2012;*
*Accepted 10 September 2012*
Available online 18 September 2012

***Keywords:***
α-helical oligomers;
nucleation;
critical concentration;
posttranslational modification;
phosphomimetic

† http://keck.med.yale.edu/ssps/
‡ http://lamar.colostate.edu/~sreeram/CDPro

***Abbreviations used:***
polyQ, polyglutamine; HD, Huntington's disease; ssNMR, solid-state NMR; WT, wild type; EM, electron microscopy; PBS, phosphate-buffered saline; FTIR, Fourier transform infrared spectroscopy; MAS, magic angle spinning.

## References

1. Zuccato, C., Valenza, M. & Cattaneo, E. (2010). Molecular mechanisms and potential therapeutical

targets in Huntington's disease. *Physiol. Rev.* **90**, 905–981.
2. Ross, C. A. & Tabrizi, S. J. (2011). Huntington's disease: from molecular pathogenesis to clinical treatment. *Lancet Neurol.* **10**, 83–98.
3. Bates, G. P. & Benn, C. (2002). The polyglutamine diseases. In *Huntington's Disease* (Bates, G. P., Harper, P. S. & Jones, L., eds), pp. 429–472, Oxford University Press, Oxford, U.K.
4. Wilburn, B., Rudnicki, D. D., Zhao, J., Weitz, T. M., Cheng, Y., Gu, X. F. *et al.* (2011). An antisense CAG repeat transcript at JPH3 locus mediates expanded polyglutamine protein toxicity in Huntington's disease-like 2 mice. *Neuron*, **70**, 427–440.
5. Davies, S. W., Turmaine, M., Cozens, B. A., DiFiglia, M., Sharp, A. H., Ross, C. A. *et al.* (1997). Formation of neuronal intranuclear inclusions underlies the neurological dysfunction in mice transgenic for the HD mutation. *Cell*, **90**, 537–548.
6. DiFiglia, M., Sapp, E., Chase, K. O., Davies, S. W., Bates, G. P., Vonsattel, J. P. & Aronin, N. (1997). Aggregation of huntingtin in neuronal intranuclear inclusions and dystrophic neurites in brain. *Science*, **277**, 1990–1993.
7. Scherzinger, E., Lurz, R., Turmaine, M., Mangiarini, L., Hollenbach, B., Hasenbank, R. *et al.* (1997). Huntingtin-encoded polyglutamine expansions form amyloid-like protein aggregates in vitro and in vivo. *Cell*, **90**, 549–558.
8. Chen, S., Berthelier, V., Yang, W. & Wetzel, R. (2001). Polyglutamine aggregation behavior in vitro supports a recruitment mechanism of cytotoxicity. *J. Mol. Biol.* **311**, 173–182.
9. Gu, X., Greiner, E. R., Mishra, R., Kodali, R., Osmand, A., Finkbeiner, S. *et al.* (2009). Serines 13 and 16 are critical determinants of full-length human mutant huntingtin induced disease pathogenesis in HD mice. *Neuron*, **64**, 828–840.
10. Gray, M., Shirasaki, D. I., Cepeda, C., Andre, V. M., Wilburn, B., Lu, X. H. *et al.* (2008). Full-length human mutant huntingtin with a stable polyglutamine repeat can elicit progressive and selective neuropathogenesis in BACHD mice. *J. Neurosci.* **28**, 6182–6195.
11. Steffan, J. S., Agrawal, N., Pallos, J., Rockabrand, E., Trotman, L. C., Slepko, N. *et al.* (2004). SUMO modification of Huntingtin and Huntington's disease pathology. *Science*, **304**, 100–104.
12. Atwal, R. S., Xia, J., Pinchev, D., Taylor, J., Epand, R. M. & Truant, R. (2007). Huntingtin has a membrane association signal that can modulate huntingtin aggregation, nuclear entry and toxicity. *Hum. Mol. Genet.* **16**, 2600–2615.
13. Rockabrand, E., Slepko, N., Pantalone, A., Nukala, V. N., Kazantsev, A., Marsh, J. L. *et al.* (2007). The first 17 amino acids of Huntingtin modulate its sub-cellular localization, aggregation and effects on calcium homeostasis. *Hum. Mol. Genet.* **16**, 61–77.
14. Thompson, L. M., Aiken, C. T., Kaltenbach, L. S., Agrawal, N., Illes, K., Khoshnan, A. *et al.* (2009). IKK phosphorylates Huntingtin and targets it for degradation by the proteasome and lysosome. *J. Cell Biol.* **187**, 1083–1099.
15. Atwal, R. S., Desmond, C. R., Caron, N., Maiuri, T., Xia, J. R., Sipione, S. & Truant, R. (2011). Kinase inhibitors modulate huntingtin cell localization and toxicity. *Nat. Chem. Biol.* **7**, 453–460.
16. Chen, S., Ferrone, F. & Wetzel, R. (2002). Huntington's disease age-of-onset linked to polyglutamine aggregation nucleation. *Proc. Natl Acad. Sci. USA*, **99**, 11884–11889.
17. Kar, K., Jayaraman, M., Sahoo, B., Kodali, R. & Wetzel, R. (2011). Critical nucleus size for disease-related polyglutamine aggregation is repeat-length dependent. *Nat. Struct. Mol. Biol.* **18**, 328–336.
18. Bhattacharyya, A., Thakur, A. K., Chellgren, V. M., Thiagarajan, G., Williams, A. D., Chellgren, B. W. *et al.* (2006). Oligoproline effects on polyglutamine conformation and aggregation. *J. Mol. Biol.* **355**, 524–535.
19. Thakur, A. K., Jayaraman, M., Mishra, R., Thakur, M., Chellgren, V. M., Byeon, I. J. *et al.* (2009). Polyglutamine disruption of the huntingtin exon 1 N terminus triggers a complex aggregation mechanism. *Nat. Struct. Mol. Biol.* **16**, 380–389.
20. Jayaraman, M., Kodali, R., Sahoo, B., Thakur, A. K., Mayasundari, A., Mishra, R. *et al.* (2012). Slow amyloid nucleation via alpha-helix-rich oligomeric intermediates in short polyglutamine-containing huntingtin fragments. *J. Mol. Biol.* **415**, 881–899.
21. Mishra, R., Jayaraman, M., Roland, B. P., Landrum, E., Fullam, T., Kodali, R. *et al.* (2012). Inhibiting the nucleation of amyloid structure in a huntingtin fragment by targeting alpha-helix-rich oligomeric intermediates. *J. Mol. Biol.* **415**, 900–917.
22. Wetzel, R. (2012). Physical chemistry of polyglutamine: intriguing tales of a monotonous sequence. *J. Mol. Biol.* **421**, 466–490.
23. Jayaraman, M., Mishra, R., Kodali, R., Thakur, A. K., Koharudin, L. M. I., Gronenborn, A. M. & Wetzel, R. (2012). Kinetically competing huntingtin aggregation pathways control amyloid polymorphism and properties. *Biochemistry*, **51**, 2706–2716.
24. Thakur, A. & Wetzel, R. (2002). Mutational analysis of the structural organization of polyglutamine aggregates. *Proc. Natl Acad. Sci. USA*, **99**, 17014–17019.
25. Jayaraman, M., Kodali, R. & Wetzel, R. (2009). The impact of ataxin-1-like histidine insertions on polyglutamine aggregation. *Protein Eng. Des. Sel.* **22**, 469–478.
26. Thakur, A. K., Yang, W. & Wetzel, R. (2004). Inhibition of polyglutamine aggregate cytotoxicity by a structure-based elongation inhibitor. *FASEB J.* **18**, 923–925.
27. Sivanandam, V. N., Jayaraman, M., Hoop, C. L., Kodali, R., Wetzel, R. & van der Wel, P. C. (2011). The aggregation-enhancing huntingtin N-terminus is helical in amyloid fibrils. *J. Am. Chem. Soc.* **133**, 4558–4566.
28. Wishart, D. S. & Sykes, B. D. (1994). The 13C chemical-shift index: a simple method for the identification of protein secondary structure using 13C chemical-shift data. *J. Biomol. NMR*, **4**, 171–180.
29. Kheterpal, I., Williams, A., Murphy, C., Bledsoe, B. & Wetzel, R. (2001). Structural features of the Ab amyloid fibril elucidated by limited proteolysis. *Biochem.* **40**, 11757–11767.
30. O'Nuallain, B., Shivaprasad, S., Kheterpal, I. & Wetzel, R. (2005). Thermodynamics of abeta(1–40) amyloid fibril elongation. *Biochemistry*, **44**, 12709–12718.

31. Williams, A. D., Shivaprasad, S. & Wetzel, R. (2006). Alanine scanning mutagenesis of Abeta(1–40) amyloid fibril stability. *J. Mol. Biol.* **357**, 1283–1294.
32. Julien, S. G., Dube, N., Hardy, S. & Tremblay, M. L. (2011). Inside the human cancer tyrosine phosphatome. *Nat. Rev. Cancer*, **11**, 35–49.
33. Luo, S., Vacher, C., Davies, J. E. & Rubinsztein, D. C. (2005). Cdk5 phosphorylation of huntingtin reduces its cleavage by caspases: implications for mutant huntingtin toxicity. *J. Cell Biol.* **169**, 647–656.
34. Schilling, B., Gafni, J., Torcassi, C., Cong, X., Row, R. H., LaFevre-Bernt, M. A. *et al.* (2006). Huntingtin phosphorylation sites mapped by mass spectrometry. Modulation of cleavage and toxicity. *J. Biol. Chem.* **281**, 23686–23697.
35. Pardo, R., Colin, E., Regulier, E., Aebischer, P., Deglon, N., Humbert, S. & Saudou, F. (2006). Inhibition of calcineurin by FK506 protects against polyglutamine-huntingtin toxicity through an increase of huntingtin phosphorylation at S421. *J. Neurosci.* **26**, 1635–1645.
36. Aiken, C. T., Steffan, J. S., Guerrero, C. M., Khashwji, H., Lukacsovich, T., Simmons, D. *et al.* (2009). Phosphorylation of threonine 3: implications for Huntingtin aggregation and neurotoxicity. *J. Biol. Chem.* **284**, 29427–29436.
37. Havel, L. S., Wang, C. E., Wade, B., Huang, B. D., Li, S. H. & Li, X. J. (2011). Preferential accumulation of N-terminal mutant huntingtin in the nuclei of striatal neurons is regulated by phosphorylation. *Hum. Mol. Genet.* **20**, 1424–1437.
38. Johnston, J. A., Ward, C. L. & Kopito, R. R. (1998). Aggresomes: a cellular response to misfolded proteins. *J. Cell Biol.* **143**, 1883–1898.
39. Waelter, S., Boeddrich, A., Lurz, R., Scherzinger, E., Lueder, G., Lehrach, H. & Wanker, E. E. (2001). Accumulation of mutant huntingtin fragments in aggresome-like inclusion bodies as a result of insufficient protein degradation. *Mol. Biol. Cell*, **12**, 1393–1407.
40. Broncel, M., Falenski, J. A., Wagner, S. C., Hackenberger, C. P. & Koksch, B. (2010). How post-translational modifications influence amyloid formation: a systematic study of phosphorylation and glycosylation in model peptides. *Chemistry*, **16**, 7881–7888.
41. Valette, N. M., Radford, S. E., Harris, S. A. & Warriner, S. L. (2012). Phosphorylation as a tool to modulate aggregation propensity and to predict fibril architecture. *ChemBioChem*, **13**, 271–281.
42. Inoue, M., Konno, T., Tainaka, K., Nakata, E., Yoshida, H. & Morii, T. (2012). Positional effects of phosphorylation on the stability and morphology of tau-related amyloid fibrils. *Biochemistry*, **51**, 1396–1406.
43. Bugg, C. W., Isas, J. M., Fischer, T., Patterson, P. H. & Langen, R. (2012). Structural features and domain organization of huntingtin fibrils. *J. Biol. Chem.* **287**, 31739–31746.
44. Dyson, H. J. (2011). Expanding the proteome: disordered and alternatively folded proteins. *Q. Rev. Biophys.* **44**, 467–518.
45. O'Nuallain, B., Thakur, A. K., Williams, A. D., Bhattacharyya, A. M., Chen, S., Thiagarajan, G. & Wetzel, R. (2006). Kinetics and thermodynamics of amyloid assembly using a high-performance liquid chromatography-based sedimentation assay. *Methods Enzymol.* **413**, 34–74.
46. Jayaraman, M., Thakur, A. K., Kar, K., Kodali, R. & Wetzel, R. (2011). Assays for studying nucleated aggregation of polyglutamine proteins. *Methods*, **53**, 246–254.
47. Sreerama, N. & Woody, R. W. (2000). Estimation of protein secondary structure from circular dichroism spectra: comparison of CONTIN, SELCON, and CDSSTR methods with an expanded reference set. *Anal. Biochem.* **287**, 252–260.